PROCEEDINGS, Thirty-Ninth Workshop on Geothermal Reservoir Engineering
Stanford University, Stanford, California, February 24-26, 2014
SGP-TR-202

Validating Models to Forecasting Induced Seismicity Related to Deep Geothermal Energy Projects

Eszter Király, Valentin Gischig, Dimitrios Karvounis and Stefan Wiemer

Swiss Seismological Service, ETH Zurich, Sonneggstrasse 5, NO H39.2, CH-8092 Zurich, Switzerland

eszter.kiraly@sed.ethz.ch

Keywords: deep geothermal systems, seismicity forecast, CSEP testing, principal components analysis, Cooper Basin, Soultz-sous-Forêts, Basel, St. Gallen

ABSTRACT

Deep geothermal systems have big potential for future green energy resources. Induced seismicity occurring during early stimulation periods in deep geothermal projects of past years, however, clearly document our limited understanding of the processes at depth that lead to significant seismic hazard and that may influence public acceptance of future projects. Managing induced seismicity related to deep geothermal projects with advanced traffic light systems require models that are forward looking, dynamically updated on the fly as new data arrive and probabilistic in the sense that the inherent uncertainties in our understanding of the processes and in the model parameters are included. Based on modeling of the 2006 Basel induced sequence, Goertz-Allmann and Wiemer (2013) and Gischig and Wiemer (2013) suggest a so-called hybrid geomechanical forecast model that loosely couples the evolving pressure perturbation at depth with a stochastic seed model of potential faults. We currently develop a fully coupled non-linear hydraulic-seismic 3D model joint with a hazard assessment procedure. The goal is to improve the forecasting ability owing to validated physical constraints. As one of the first steps, a forecast testing center is being built up and comparison of observed co- and post-stimulation seismicity (maximum magnitude, productivity, b-value, seismogenic index, spatial parameters) is carried out for various deep geothermal stimulation projects. We also report on the ongoing efforts to analyze the 2013 St. Gallen earthquake sequence where more than 700 earthquakes related to this project have been recorded to date, the largest one having a magnitude $m_w = 3.3$. This project also pointed out our current limited understanding on complex processes of reservoir behavior, for instance the potential role of over-pressured methane gas in inducing earthquakes.

1. INTRODUCTION

Due to the phase out of nuclear energy production in Switzerland by 2034, increasing efforts has been initiated on renewable energy resources, especially on deep geothermal energy, since this type of energy has potential to contribute to long-term energy resources.

Among various types of deep geothermal reservoirs two end member types of geothermal reservoir can be distinguished: (1) hydrothermal systems, where sufficient amount of hot water circulates through a highly permeable medium and (2) petrothermal systems where the hot rock reservoir has low permeability and small quantity of fluid is present. Hydrothermal systems are quite rare, usually bound to volcanic regions. Petrothermal systems, in contrast are considered to be independent of geological site conditions. In case of low permeability, the reservoir needs to be created (i.e. permeability has to be enhanced), so that fluid can circulate in a closed loop. These engineered reservoirs are called Enhanced Geothermal System (EGS). Permeability enhancement in EGS is usually done with high pressure stimulations with water or acidic fluid. Process of enhancing permeability is associated with seismic events that are usually micro-earthquakes ($m < 3.0$), but also larger events can occur such as magnitude 4 - 5. Felt earthquakes raises public concerns about geothermal projects.

During the last decades two geothermal projects have been launched in Switzerland. In the north-western part, near Basel a reservoir was stimulated at about 5 km depth during 6 days in Dec 2006. During the injection some earthquakes were felt by the population, but the main shock ($m_L = 3.4$) occurred after shut-in and followed by three aftershocks of $m_L > 3.0$ (Häring et al., 2008), which finally resulted in closing the project.

The other project was started in 2007 in the eastern part of Switzerland near St. Gallen. The project is still running. A pre-existing fault was explored by seismic imaging techniques and targeted around a karstic Mesozoic limestone formation. After drilling to the fault, acidization was carried out in order to enhance the permeability between the formation and the well in July 2013. This procedure led to leakage of gas pockets trapped beneath impervious sedimentary layers. Due to the high well-head pressure borehole blow-out was impending and operators decided to control the well with injection of muddy fluid. This resulted in increased seismicity with a main shock of $m_w = 3.3$. After several weeks a production test was accomplished with very low seismic activity (Kraft et al., 2013).

These projects have also showed that operators must find a balance between reservoir creation that leads to economically profitable geothermal systems and induced seismicity. In order to avoid large seismic events, and control the reservoir creation a dynamically updated warning system is needed, that is able to forecast seismicity for short (a few hours, days) and long-terms (weeks, months).

In this paper, we report on the new steps towards modeling and forecasting of induced seismicity, which can help on-site decision-making in the future, and show a preliminary comparison of four deep geothermal datasets (Cooper Basin 2003, Soultz-sous-Forêts 2004, Basel 2006, St. Gallen 2013) in terms of temporal and spatial variation of the seismicity.

2. FORECASTING SEISMIC HAZARD DURING AND AFTER STIMULATION BASED ON OBSERVED SEISMICITY AND HYDRAULIC DATA

2.1 Introduction – State of the Art

The key element of reservoir design schemes avoiding large induced earthquakes is the ability of reacting on not yet occurred but potentially foreseen seismic events. To be able to do so (and improve traditional static warning systems), a multidisciplinary project has been started to develop the Advanced Traffic Light and Assessment System for Induced Seismicity (e.g., Bachmann et al., 2011; Mena et al., 2013; Goertz-Allmann and Wiemer, 2013). Several models have been developed to date, some of which are statistical models (e.g., Reasenberg and Jones, 1989; Hainzl, 2005; Bachmann et al., 2011; Mena et al., 2013) while others are physics-based numerical models (e.g., Bruel, 2005; Kohl and Mégel, 2007; Baisch et al., 2010; Rutqvist, 2011; McClure and Horne, 2012; Wang and Ghassemi, 2012; Karvounis, 2013). Statistical models are simple, quick and give reasonable seismicity forecast (Mena et al., 2013). However, they do not model permeability creation, do not account for the governing physical processes, they can give good constrains only for the time period when data is available, and forecasts do not perform sufficiently well for longer time periods. Moreover, they are not able to capture unexpected events (e.g., large magnitudes). Thus, they have limited capabilities for investigation of long-term intervals, post-shut-in behavior or alternative injection scenarios.

The main advantage of physics-based models is due to the fact that they reasonably represent the underlying physical processes. Hence, they have the capability to improve the forecast for longer time periods, to predict unexpected events and to study phenomena with sensitivity analyses (scenarios). However, they do not necessarily account for epistemic uncertainties (i.e., uncertainty due to lack of knowledge or data) and aleatory variabilities (i.e., intrinsic randomness of a phenomenon). Moreover, due to their computational expenses they cannot be applied in near-real time. Thus, no comprehensive physics-based model exists to date that can be used in an induced seismic hazard assessment framework.

An attempt to exploit advantages of statistical models (efficiency) and physics-based models (physical process representation) are so-called hybrid models as described by Goertz-Allmann and Wiemer (2013). They developed a geomechanical forward model called the GeoMechanical Seed model (GMS), where seed points (potential earthquake nucleation points) are randomly placed in a heterogeneous stress field. Heterogeneity is modeled by assigning minimum and maximum stresses with a mean corresponding to the in-situ stress estimates and a normal distributed perturbation with a standard deviation of 10% about the mean. Then, a corresponding b-value (i.e., ratio between large and small magnitude events) is given to each seed point following a linear relationship between differential stress and b-value. Rupture initiation at seeds occurs due to simple, homogeneous, isotropic pore pressure diffusion. Earthquake triggering is governed by the Coulomb failure criterion. Magnitudes of triggered earthquakes are randomly drawn from a Gutenberg-Richter distribution (Gutenberg and Richter, 1944) of a corresponding local b-value. Once an earthquake has occurred a new stress state is assigned to the seed point through a static stress drop tied to the normal failure stress. This characteristic of the model allows re-triggering of earthquakes if pressure evolution further increases.

Gischig and Wiemer (2013) made one step further towards hybrid models: earthquakes are triggered by a pressure field that is based on non-linear pressure diffusion with irreversible permeability enhancement instead linear pressure diffusion. The model is an improved version of the first GMS model but share the main concept: hydraulics and seismicity are coupled only in one direction. Hydraulic properties come from inversion of time dependent wellhead pressure curve. The pressure field then gives the input for the seismic seed model inherited from Goertz-Allmann and Wiemer (2013). The radially symmetric pressure diffusion was solved by a 2D model with squared geometry in the COMSOL simulation software. Best fit parameters both in hydraulics and seismicity parts were found by Monte Carlo search. The model was able to reproduce the spatio-temporal variation of the seismicity cloud, seismicity rates at different magnitudes, as well as the observation that seismic hazard remains high after shut-in in the case of the Basel geothermal project.

In order to model more precisely the reservoir creation processes and establish the Advanced Traffic Light and Assessment System for Induced Seismicity our group currently develops a fully coupled non-linear hydraulic-seismic 3D model joint with the hazard assessment procedure.

2.2 Model Performance Testing and Ranking

As one of the first steps, a testing framework for induced seismicity forecasting is being built up. The aim is to balance model prediction performance and model complexity. In other words, we seek to answer the question: is a certain degree of model complexity necessary to forecast micro-seismicity and unexpected, large events well, or does it only increase model complexity without giving better results?

Forecasting consists of two time intervals: a learning and a forecast period. During the learning period models can „learn“ about the actual dataset, and then give an estimation of the particular process for the (near) future, i.e. the forecast period. In the context of seismicity, during the learning period a certain number of seismic events are observed, analyzed according to their distribution in space, time and magnitude. Then a calibrated model forecasts the number of events, their magnitudes and approximate location for a given time interval in the future. Classical seismic forecasts give the location of the earthquakes in latitude-longitude position and the order of magnitude of forecast time period is years. However, for induced seismic events in geothermal systems, the vertical component of an event location plays an important role, thus 3D position of the events is needed. Additionally, the forecast period must be at the order of hours, days for short-term, weeks or months for long-term forecasts.

Forecast tests are carried out using the guidelines of the Collaboratory for the Study of Earthquake Predictability (CSEP, http://www.cseptesting.org/centers/eth). First, one has to study if the model is consistent with the data. Several tests can be applied, such as, Number-test (i.e., number of forecast events compared to observed earthquakes), Likelihood-test (i.e., test the overall consistency of forecast with the observation), Magnitude-test (i.e., comparison of magnitudes of forecast and observed events) and Space-test (i.e., comparison of spatial distribution of forecast and observed events) (Zechar, 2010). In order to rank the models, the Student's paired t-test (Student, 1908) and of Wilcoxon signed-rank test (Wilcoxon, 1945) are used. These tests allow only for ranking forecasts, however, cannot give an absolute score to each model (Eberhard et al., 2012).

Models that have been or will be tested in the induced seismicity context are the followings:

1. Epidemic Type Aftershock Sequence (ETAS) model (Hainzl, 2005), background seismicity depends on the injected flow
2. Shapiro model based on seismogenic index calculation (Shapiro et al., 2010)
3. GeoMechanical Seed model (GMS-1) with linear flow (Goertz-Allmann and Wiemer, 2013)
4. GeoMechanical Seed model (GMS-2) with non-linear flow (Gischig and Wiemer, 2013)

Complexity is increasing from model 1 towards model 4. ETAS model takes into account exclusively seismicity: each seismic event triggers its own aftershock sequence, which decays following the Omori-Utsu law. Shapiro model uses both seismic and hydraulic data. The model is based on a site specific parameter, the so-called seismogenic index (Shapiro et al., 2010), which is an estimation of the potential seismic response of the given site. It can be calculated from a short injection period as well as from the whole stimulation taking into account the b-value of the observed seismicity, the cumulative number of earthquakes above a certain magnitude threshold (here we use m >= 1) and the total injected fluid volume. High seismogenic index points out sites with high seismic activities compared to total injected volume. This value allows not only a relative comparison between the seismic responses of geothermal sites but also prediction of the number of events within a specific magnitude range. On the one hand, ETAS and Shapiro models are quick, on the other hand, they do not account for spatial variations of the seismicity could.

GMS-1 and GMS-2 involve hydraulic and seismic processes in a 3D space, their coupling however is very loose, hydraulic and seismic processes are treated separately. The testing of these models using the aforementioned testing framework will be subject of future work as soon as both the hydraulic and the seismic component are well calibrated against real observations. As it was mentioned before, our group works on the development of fully coupled seismic-hydraulic models. Although, none of them are calibrated, thus not available for forecast testing for the time being, it would be worth to test them within the same framework in future.

First steps are made towards the implementation of Shapiro model. Similarly to Mena et al (2013) we calibrate the model using learning periods that grow with time intervals of six hours. Seismicity rates are then forecasted for the subsequent six-hour bins. This is done for a 15-day period starting from the fluid injection. This model gives only the number of earthquakes in separate magnitude bins but could not predict the location of the seismic events. In order to place forecasted events in 3D, we integrate spatial kernels into the model. We currently work on the construction of the kernels applying principal component analysis (PCA) of the gradually growing seismicity cloud. We are interested in the centroid position of the seismic cluster, the orientation and the length of principal axes in six-hour steps. This allows us to construct a dynamic 3D spatial model of the seismicity density (i.e. number of events per volume) in the target region. The forecasted events are placed according to the modeled seismicity density. Since during stimulations the seismicity is quite high near the well and decays toward the borders of the reservoir, as a first approach, we assume Gaussian distribution of the seismicity centered around the injection point. Many projects showed that the behavior of the seismicity changes after shut-in: only few seismic events are observed in the direct vicinity of the injection point, whereas seismicity concentrates towards the borders of the reservoir (Kaiser effect). Due to this phenomenon the spatial kernel has to be changed after shut-in.

Primarily all tests are carried out using the Basel 2006 dataset. However, to explore a realistic kernel we investigated the spatial evolution of other deep geothermal reservoirs, such as Cooper Basin 2003, Soultz-sous-Forêts 2004 and St. Gallen 2013. The next section presents a preliminary comparative analysis of these four datasets.

3. COMPARISON OF SEISMIC DATASETS IN FOUR GEOTHERMAL PROJECTS

3.1 Overview of projects

This section briefly summarizes the main geological site conditions and milestones of the Cooper Basin 2003, Soultz-sous-Forêts 2004, Basel 2006 and St. Gallen 2013 geothermal project.

3.1.1 Cooper Basin

The Cooper Basin geothermal site is located close to Innamincka, Moomba, South Australia (Hunt and Morelli, 2006). The granitic basement is overlain by 3.6 km sediments (Majer et al., 2007). According to the World Stress Map, regional tectonic setting shows a transition from a thrust fault to a strike-slip regime (Zoback, 1992). Orientation of the main horizontal stress is E-W. The natural temperature is about 250°C at 4.4 km depth (Baisch et al., 2006) where porosity and permeability are low (Chen and Wyborn, 2006). The reservoir is critically stressed (Hunt and Morelli, 2006). The Habanero-1 injection well was drilled in the early 2000s. The well is 4400m deep, outflow zone is at 4250 m depth corresponding to the location of the main fracture zone (Majer et al., 2007; Chen and Wyborn, 2006). In this work we use the dataset of the first stimulation carried out in the well of Habanero-1 between November-December in 2003.

3.1.2 Soultz-sous-Forêts

The Soultz-sous-Forêts geothermal site is located between Kutzenhausen and Soultz-sous-Forêts in the Upper Rhine Graben, about 70km north from Strasbourg in Alsace (France). The stress regime is normal faulting roughly N-S striking (Zoback, 1992). The geothermal gradient is about 100°C/km within the 1.5 km thick sedimentary cover over a granitic basement (Evans et al., 2012). This abnormally high geothermal gradient is most probably due to deep hydrothermal convection cells in the fractured basement (Gérard et al., 2006). The geothermal project started in the early 1980s. During almost 30 years, 4 wells were drilled into two reservoirs: a shallower reservoir at about 3.5 km depth (GPK1, GPK2 wells), deeper reservoir at about 4.5 km (GPK2, GPK3, GPK4 wells). Several stimulations and circulation test were carried out. Energy production has started in 2008. In this work we used the stimulation dataset of September 2004.

3.1.3 Basel

The Basel geothermal site is located at the south-eastern margin of the Upper Rhine Graben, in north-western Switzerland. The graben structure is oriented in NNE-SSW direction. The granitic basement is covered by 2.4 km sedimentary rocks. The well Basel 1 was drilled to the depth of 5 km between May and October in 2006. After several tests, the reservoir was hydraulically stimulated to enhance the permeability in December 2006. The plan was to stimulated during 21 days, but after 6 days the injection was stopped due to intensive seismicity including event magnitudes up to $m_L = 2.6$. Five hours after the well shut-in, a $m_L = 3.4$ event occurred, followed by three aftershocks of $m_L > 3.0$ (Häring etal., 2008). Based on the results of a subsequent risk study, it was decided to abandon the project. Dataset of this project is one of the best quality datasets of geothermal systems to date.

3.1.4 St. Gallen

The St. Gallen geothermal site is located in north-eastern Switzerland, about 5 km west from the city of St. Gallen. The stress regime includes local extension observed along strike-slip faults. According to (Singer et al., in prep) the stress field is the local expression of the active convergence of the European and Adriatic plate to the North of the Alpine front.

A fault at 4-5 km depth in the Malm formation below the 4 km-thick molasse (revealed by 3D seismic campaign) was targeted to use existing high permeability. Temperature at that depth is about 200°C (GeowattAG 2009). The Swiss Seismological Service (SED) started seismic monitoring with 7 surface and 1 borehole stations in 2012, and another 7 stations installed in July 2013. Drilling operations started in March 2013 (Kraft et al., 2013).

After having drilled into the fault system, an injection test was carried out (14th July). Then acid working fluid was pumped into the well accompanied by low seismicity rate (17th July) in order to enhance the connection between the well and the formation. On 19th July gas flow was observed in the well, which resulted in increasing well-head pressure. To control the well, heavy mud was injected, which increased seismic activity. However, to ensure well safety, injection could not be stopped. Due to the injection of about 700m³ working fluid about 700 earthquakes were recorded with a main shock of $m_w = 3.3$ (20th July 3:30am). The event was followed by rapid decrease of well-head pressure, steady mud loss and gas entry (Kraft et al., 2013). More than 340 events were relocated with double difference method highlighting a clear lateral structure in the Mezozoic sediments below the openhole (Diehl et al 2013).

A production test was carried out in November 2013, during which very little seismicity occurred. Stakeholders called for risk study, decision on the project future will be made in September 2014 (Kraft et al., 2013).

3.2 Comparison of Seismic Datasets

The magnitude distribution of the overall seismicity is described by the magnitude-frequency distribution (FMD), where the logarithm of the cumulative number of events is displayed against magnitudes (figure 1). Following the Gutenberg-Richter law (Gutenberg and Richter 1944), a power law is fitted to each dataset. The slope of the fitted line gives the b-value, the intercept with the vertical axis is the a-value, also termed productivity.

For comparison, all datasets are cut at the end of 12 days after the injection had started. Seismicity of Soultz 2004 and Cooper Basin 2003 stimulations shows similar behavior in terms of both productivity and overall b-value. Seismicity in Basel indicates a higher b-value, in other words small amount of high magnitudes compared to lower ones, and also high productivity. The maximum observed magnitude is $m_w = 3.0$, which is less than that of St. Gallen 2013 ($m_w = 3.3$). St. Gallen 2013 stimulation shows an intermediate b-value after 12 days with almost the same productivity as Cooper Basin 2003 and Soultz 2004. If we take into account hydraulic data and normalize the cumulative number of events with the total injected volume, the FMD of St. Gallen 2013 changes (figure 1b). Its productivity becomes significantly higher than Soultz 2004 and Cooper Basin 2003. Productivity of Basel stays quite high even after normalization. This suggests that the site is seismically reactive with respect to the amount of injected fluid volume. Soultz 2004 and Cooper Basin 2003 datasets show again very similar behavior.

The evolution of the seismogenic index (figure 2a) shows that the values usually stabilize after shut-in; in the case of Soultz 2004 and Cooper Basin 2003 it is stable even during the stimulation. In contrast, seismogenic index at St. Gallen 2013 is still unstable 2 days after shut-in. The difference between the value at shut-in and after 12 days is 0.5. The stable value of the seismogenic index at St. Gallen is higher than that of Basel, which indicates more seismic activity compared to the injected volume. In the case of Cooper Basin 2003 and Soultz 2004, a larger amount of total injected volume is counter-balanced by smaller amount of earthquakes ($m >= 1$). Due to stable b-values, fluctuations of the seismogenic index are small. The absolute values of these seismogenic indexes are lower than those of the Swiss projects.

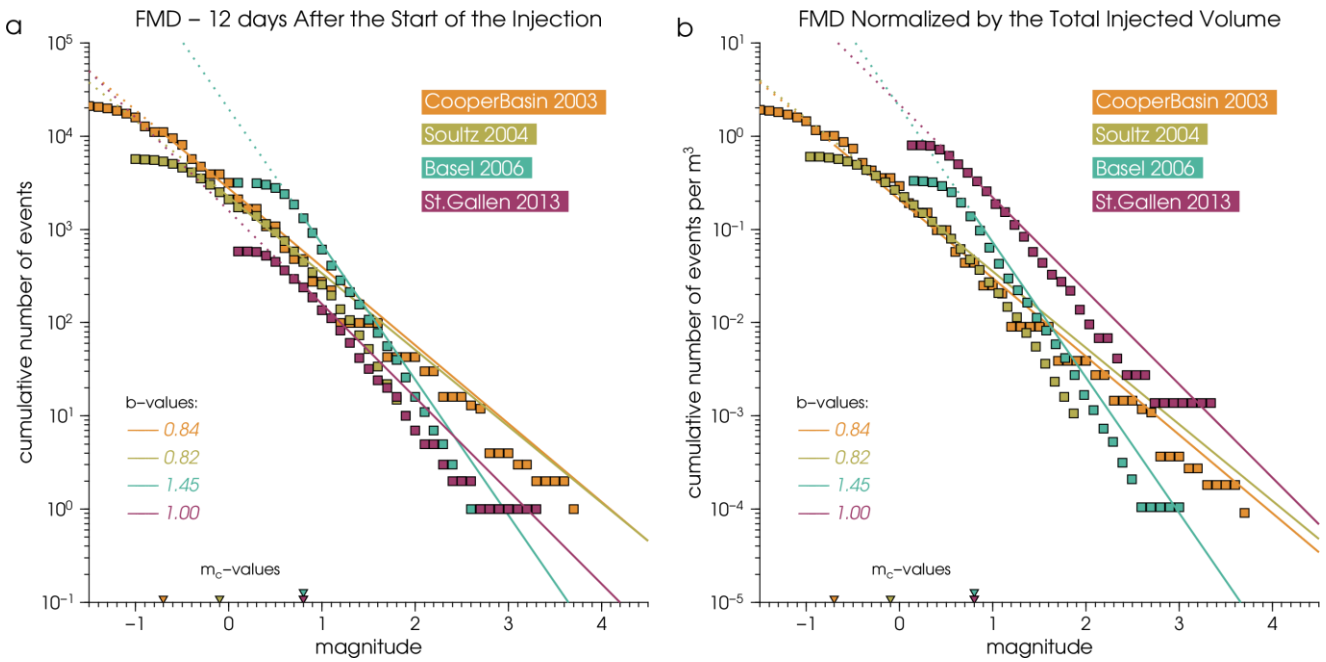

Figure 1: a) Cumulative number of events in 0.1 magnitude bins of the first 12 days of seismicity after the start of the injection in Cooper Basin 2003, Soultz-sous-Forêts 2004, Basel 2006 and St. Gallen 2013 geothermal projects. b) Cumulative number of events normalized by the total injected volume in 0.1 magnitude bins for the same projects and time interval.

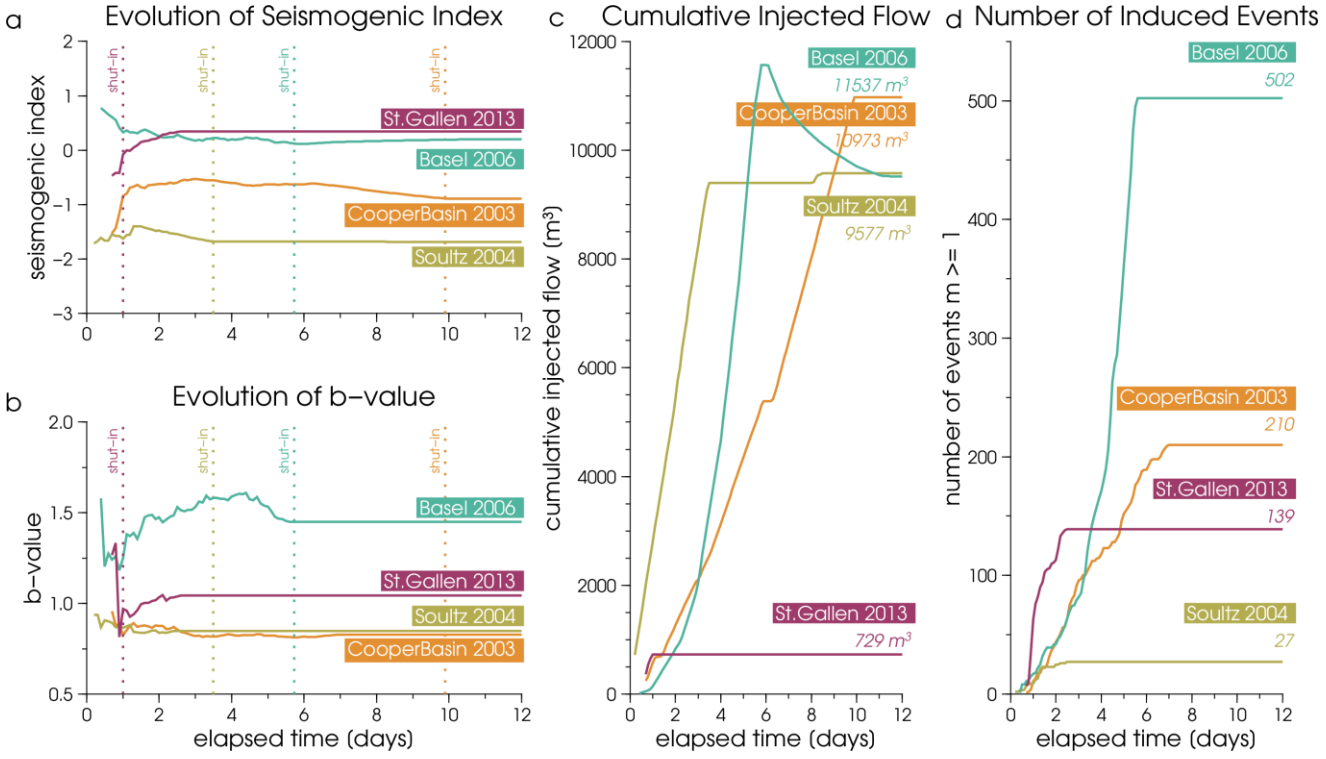

Figure 2: a) Evolution of seismogenic index during the first 12 days after the start of the injection at Cooper Basin 2003, Soultz-sous-Forêts 2004, Basel 2006 and St. Gallen 2013 geothermal projects. These values are calculated from the corresponding b-values, cumulative volume of injected fluid and total number of events m >= 1. Dotted lines indicate the shut-in time with the corresponding colors. b) Evolution of b-value for the same projects and time interval. Dotted lines indicate the shut-in time with the corresponding colors. c) Cumulative volume of injected fluid for the same projects and time interval. d) Cumulative number of earthquakes m >= 1 for the same projects and time interval.

In order to investigate the temporal evolution of the spatial properties of the seismic cloud, principal component analysis (PCA) is shown on figure 3. We calculate the orientation, length of the principal axes (eigenvectors) and the centroid position of the seismic cloud that grows gradually with six-hour steps. Changes of orientation of eigenvectors compared to the first orientation (after the first 6

hours) are shown on figure 3a, c, e, g for Cooper Basin 2003, Soultz 2004, Basel 2006, St. Gallen 2013 projects, respectively. Assuming Gaussian distribution of the events, 2σ length in each principal axis orientation is calculated which covers the 95% of the seismicity (shown on figure 3b, d, f, h for Cooper Basin 2003, Soultz 2004, Basel 2006, St. Gallen 2013 projects, respectively). Centroid locations do not vary significantly, variations are in the range of location uncertainties of the seismic events. In these four cases, the first order picture is that orientations of eigenvectors fluctuate and the lengths of the principal axes grow during stimulation, however both orientation and length of eigenvectors are stable after shut-in. An exception can be observed in case of Basel 2006: the length of the largest principal component still grows after shut-in and stabilizes approximately 2 days after. The final shape of Cooper Basin 2003 seismicity is highly elongated, Soultz 2004 perform a less elongated ellipsoid form similarly to Basel 2006. St. Gallen 2013 is characterized by a single preferred orientation in the lateral structure (figure 4).

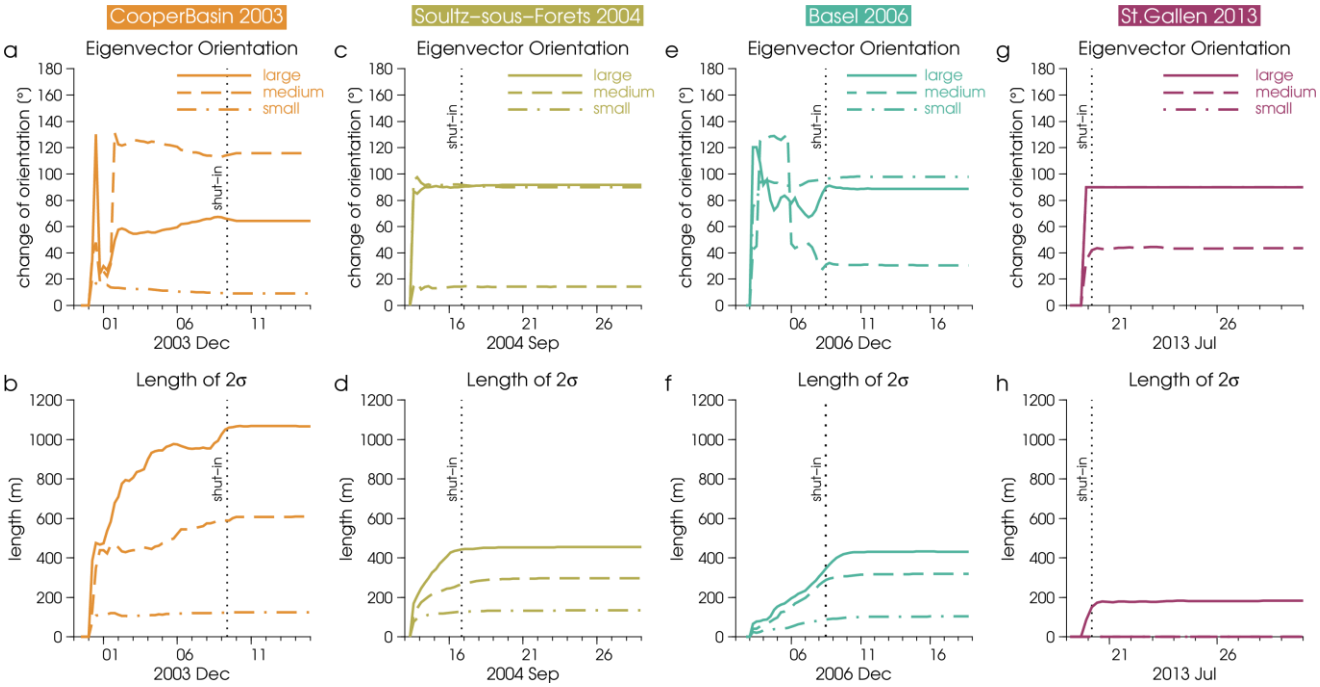

Figure 3: a) Change of eigenvector (principal axes) orientations of the gradually growing seismic cloud in Cooper Basin 2003 compared to the first eigenvector orientations (based on the seismicity 6 hours after the start of the injection). Solid, dashed and dash-dot lines correspond to large, medium and small principal axes, respectively. Dotted line indicates the shut-in time. b) Evolution of the length of the principal axes in Cooper Basin 2003 assuming Gaussian spatial distribution. 2σ length corresponds to the 95% of the actual seismicity. Dotted line indicates the shut-in time. c), e) and g) Same as a) for Soultz-sous-Forêts 2004, Basel 2006 and St. Gallen 2013, respectively. d), f) and h) Same as b) for Soultz-sous-Forêts 2004, Basel 2006 and St. Gallen 2013, respectively.

In conclusion, as a first order approach a Gaussian spatial kernel is used during stimulation period in order to forecast seismic event locations. After shut-in, however, the Kaiser effect and the observed stabilization of the extent of the seismic cloud suggest changing the kernel to an ellipsoid shell around the borders of the reservoir.

4. CONCLUSIONS

We currently develop a forecast testing center following the guidelines of the CSEP test center with the goal to compare and rank different models for induced seismicity. At the moment, four models are available for testing: ETAS, Shapiro, GMS-1 and GMS-2 models. To be able to estimate the location of forecasted events, spatial kernels must be given to those models, which do not account for spatial variations. In order to develop reasonable spatial kernels, a comparison of observed co- and post-stimulation seismicity have been carried out for four deep geothermal projects: Cooper Basin 2003, Soultz-sous-Forêts 2004, Basel 2006, St. Gallen 2013. The principal component analysis showed that orientations of eigenvectors fluctuate and the lengths of the principal axes grow during stimulation, however both orientation and length of eigenvectors are stable after shut-in. The spatial variation of the seismicity can be described by a 3D Gaussian kernel during stimulation. Taking into account the Kaiser effect and the observed stabilization of the extent of the seismic cloud suggest changing the kernel to an ellipsoid shell around the borders of the reservoir after stimulation periods.

5. ACKNOWLEDGEMENT

We acknowledge the GEOTHERM-2 project (http://www.cces.ethz.ch/projects/nature/geotherm-2) for funding this PhD. We thank the St. Galler Stadtwerke (SGSW) and Toni Kraft for providing the data of the St. Gallen geothermal project, Tobias Diehl for the relocated event coordinates. Generic Mapping Tool (GMT) was used to create all figures (http://gmt.soest.hawaii.edu). We would like to thank Stefan Hiemer for his assistance to figure 1.

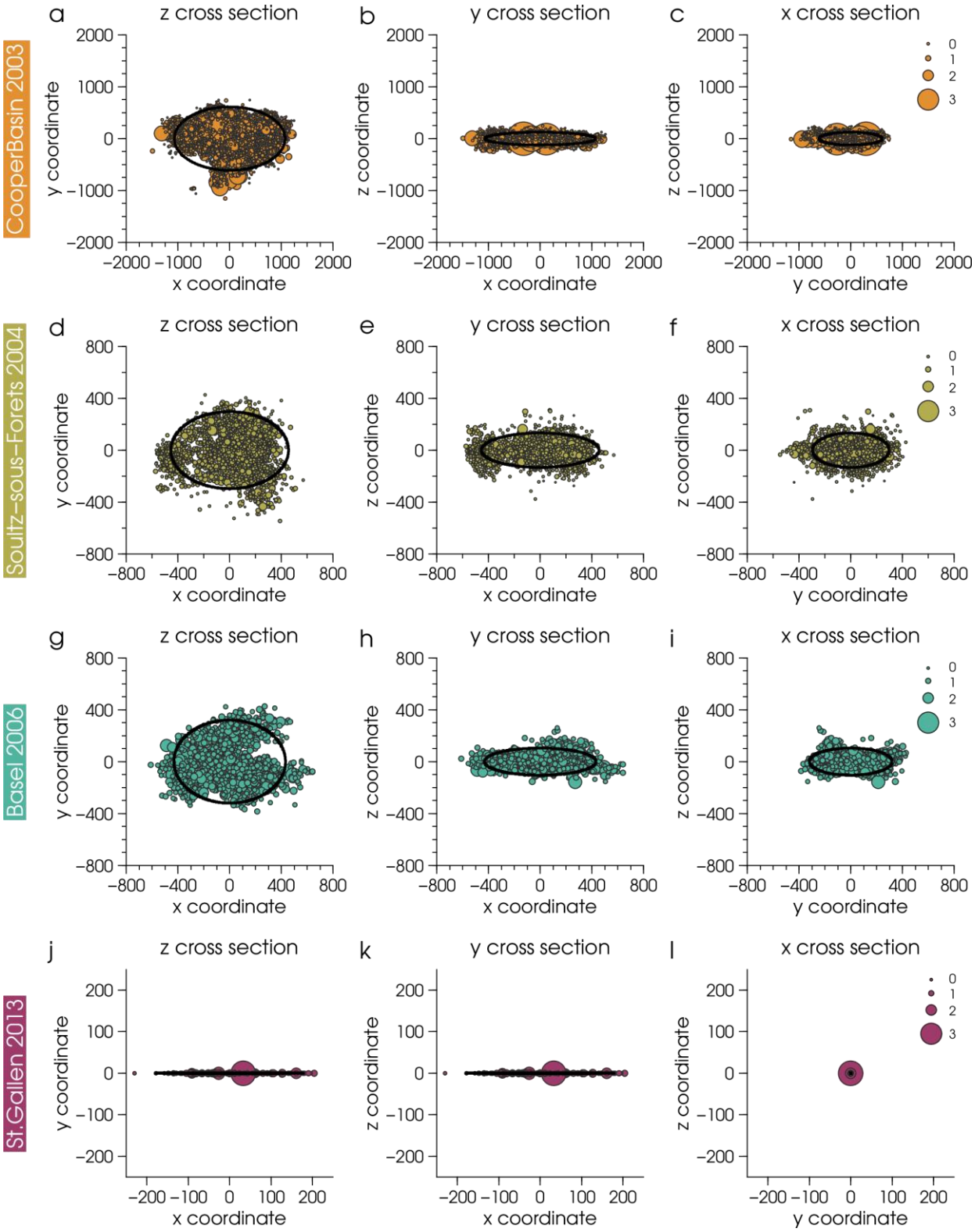

Figure 4: a) Z cross sections of the Cooper Basin seismicity rotated into the directions of principal axes. Data are cut 12 days after the start of the injection. Event magnitudes are proportional to the sizes of symbols. Solid black ellipse indicates projection of the ellipsoid, which covers the 95% of the seismicity cloud. b) Same as a) showing the y cross section and the corresponding ellipsoid projection. c) Same as a) showing the x cross section and the corresponding ellipsoid projection. d), g) and j) Same as a) for Soultz-sous-Forêts 2004, Basel 2006 and St. Gallen 2013, respectively. e), h) and k) Same as b) for Soultz-sous-Forêts 2004, Basel 2006 and St. Gallen 2013, respectively. f), i) and l) Same as c) for Soultz-sous-Forêts 2004, Basel 2006 and St. Gallen 2013, respectively. Note that size of seismicity clouds is significantly different.

REFERENCES

Bachmann, C. E., Wiemer, S., Woessner, J., and Hainzl, S. (2011). Statistical analysis of the induced Basel 2006 earthquake sequence: introducing a probability-based monitoring approach for Enhanced Geothermal Systems. *Geophysical Journal International*, **186**(2):793–807.

Baisch, S., Vörös, R., Rothert, E., Stang, H., Jung, R., and Schellschmidt, R. (2010). A numerical model for fluid injection induced seismicity at Soultz-sous-Forêts. *International Journal of Rock Mechanics and Mining Sciences*, **47**(3):405–413.

Baisch, S., Weidler, R., Voros, R., Wyborn, D., and de Graaf, L. (2006). Induced Seismicity during the Stimulation of a Geothermal HFR Reservoir in the Cooper Basin, Australia. *Bulletin of the Seismological Society of America*, **96**(6):2242–2256.

Bruel, D. (2005). Using the Migration of Induced Micro-Seismicity as a Constraint for HDR Reservoir Modelling. *In Thirtieth Workshop on Geothermal Reservoir Engineering*, pages 1–7.

Chen, D. and Wyborn, D. (2009). Habanero Field Tests in the Cooper Basin, Australia: A Proof-of-Concept for EGS. *Technical report*.

Diehl, T., Kraft, T., Kissling, E., Deichmann, N., Wiemer, S., Clinton, J., Haslinger, F., and Waldhauser, F. (2013). Near-real-time high-precision relocation of induced seismicity in the geothermal system below Sankt Gallen (Switzerland). *AGU 2013*

Eberhard, D. a. J., Zechar, J. D., and Wiemer, S. (2012). A prospective earthquake forecast experiment in the western Pacific. *Geophysical Journal International*, **190**(3):1579–1592.

Evans, K. F., Zappone, A., Kraft, T., Deichmann, N., and Moia, F. (2012). A survey of the induced seismic responses to fluid injection in geothermal and CO2 reservoirs in Europe. *Geothermics*, **41**:30–54.

Geowatt AG, Z., Support, Foralith Drilling AG, S., Dr. Roland Wyss GmbH, F., Dr. Heinrich Naef - Büro für angewandte Geologie & Kartografie, S., and Progeo GmbH, W. (2009). Mach- barkeitsstudie Tiefengeothermie Stadt St . Gallen Konzept für die Entwicklung (Planung und Erstellung) einer Geothermieanlage in der Stadt St. Gallen. *Technical Report*.

Gérard, A., Genter, A., Kohl, T., Lutz, P., Rose, P., and Rummel, F. (2006). The deep EGS (Enhanced Geothermal System) project at Soultz-sous-Forêts (Alsace, France). *Geothermics*, **35**(5-6):473–483.

Gischig, V. S. and Wiemer, S. (2013). A stochastic model for induced seismicity based on non-linear pressure diffusion and irreversible permeability enhancement. *Geophysical Journal International*. **194**(2), 1229-1249.

Goertz-Allmann, B. P. and Wiemer, S. (2013). Geomechanical modeling of induced seismicity source parameters and implications for seismic hazard assessment. *Geophysics*, **78**(1):KS25– KS39.

Gutenberg, B. and Richter, C. (1944). Frequency of Earthquakes in California. *Bulletin of the Seismological Society of America*, **34**:185 – 188.

Hainzl, S. (2005). Detecting fluid signals in seismicity data through statistical earthquake modeling. *Journal of Geophysical Research*, **110**(B5):B05S07.

Häring, M. O., Schanz, U., Ladner, F., and Dyer, B. C. (2008). Characterisation of the Basel 1 enhanced geothermal system. *Geothermics*, **37**(5):469–495.

Hunt, S. P. and Morelli, C. (2006). Cooper Basin HDR hazard evaluation: Predictive modeling of local stress changes due to HFR geothermal energy operations in South Australia. *Technical Report*.

Karvounis, D. C. (2013). Simulations of Enhanced Geothermal Systems with an Adaptive Hierarchical Fracture Representation. PhD Dissertation, ETH No. 21222.

Kohl, T. and Mégel, T. (2007). Predictive modeling of reservoir response to hydraulic stimulations at the European EGS site Soultz-sous-Forêts. *International Journal of Rock Mechanics and Mining Sciences*, **44**(8):1118–1131.

Kraft, T., Wiemer, S., Deichmann, N., Diehl, T., Edwards, B., Guilhem, A., Haslinger, F., Kiraly, E., Kissling, E., Mignan, A., Plenkers, K., Roten, D., Seif, S., and Woessner, J. (2013). The ML3.5 induced earthquake sequence at Sankt Gallen, Switzerland. *AGU 2013*

Majer, E. L., Baria, R., Stark, M., Oates, S., Bommer, J., Smith, B., and Asanuma, H. (2007). Induced seismicity associated with Enhanced Geothermal Systems. *Geothermics*, **36**(3):185–222.

McClure, M. W. and Horne, R. N. (2012). Investigation of injection-induced seismicity using a coupled fluid flow and rate / state friction model. *Geophysics*, **76**(6):WC181 – WC198.

Mena, B., Wiemer, S., and Bachmann, C. (2013). Building Robust Models to Forecast the Induced Seismicity Related to Geothermal Reservoir Enhancement. *Bulletin of the Seismological Society of America*, **103**(1):383–393.

Reasenberg, P. A. and Jones, L. M. (1989). Earthquake Hazard After a Mainshock in California. *Science*, **243**:1173 – 1176.

Rutqvist, J. (2011). Status of the TOUGH-FLAC simulator and recent applications related to coupled fluid flow and crustal deformations. *Computers & Geosciences*, **37**(6):739–750.

Shapiro, S. A., Dinske, C., Langenbruch, C., and Wenzel, F. (2010). Seismogenic index and magnitude probability of earthquakes induced during reservoir fluid stimulations. *The LeadingEdge- Special Section: Microseismic*, pages 304–309.

Singer, J., Diehl, T., Husen, S., and Kissling, E. (in prep). Alpine lithosphere slab-roll back causing lower crustal seismicity in northern foreland.

Student (1908). The Probable Error of a Mean. *Biometrika*, **6**(1):1 – 25.

Wang, X. and Ghassemi, A. (2012). A 3D Thermal-Poroelastic Model for Geothermal Reservoir Stimulation. *In 37th workshop on Geothermal Reservoir Engineering*, pages 1–11.

Wilcoxon, F. (1945). Individual Comparisons by Ranking Methods. *Bulletin Biometrics*, **1**(6):80– 83.

Zechar, J. D. (2010). Evaluating earthquake predictions and earthquake forecasts : a guide for students and new researchers. *Community Online Resource for Statistical Seismicity Analysis*, (September):1–27.

Zoback, M. L. (1992). First- and second-order patterns of stress in the lithosphere: The World Stress Map Project. *Journal of Geophysical Research*, **97**(B8):11703.